# The Influence of Thickness of Stearic Acid Self-Assembled Film on Its Protective Properties

**Zana Hajdari Gretić,[a] Ekatarina Kristan Mioč,[a] Vida Čadež,[b] Suzana Šegota,[b] Helena Otmačić Ćurković,[a,*,z] and Saman Hosseinpour[c,z]**

[a]*Department of Electrochemistry, Faculty of Chemical Engineering and Technology University of Zagreb, 10000 Zagreb, Croatia*
[b]*Division of Physical Chemistry, Ruder Bošković Institute, 10000 Zagreb, Croatia*
[c]*Max Planck Institute for Polymer Research, 55128 Mainz, Germany*

Self-assembled mono- and multilayers of stearic acid have been examined as corrosion protection systems for copper-nickel alloy in 3% sodium chloride solution. We found that self-assembled multilayers of stearic acid provide more efficient and durable corrosion protection to copper-nickel alloy than just a single monolayer. Electrochemical techniques, such as potentiodynamic polarization and electrochemical impedance spectroscopy, were used to determine the protective properties of the stearic acids films. Sum frequency generation spectroscopy, atomic force microscopy, contact angle measurements and ellipsometry were used to evaluate structural properties and thickness of the surface layers. It was found that the increase of corrosion protection from mono- to multilayer films depends on the number of layers that are formed but also on their homogeneity.
 [DOI: 10.1149/2.1461614jes] 

Manuscript submitted August 17, 2016; revised manuscript received November 18, 2016. Published November 30, 2016.

Self-assembled monolayers (SAMs) of long-chain organic compounds have are essential in many fields,[1] among other in corrosion protection.[2] In order to achieve efficient corrosion protection, self-assembled monolayers should be dense, ordered and defect free to act as a barrier against aggressive ions diffusion toward metal surface. SAMs should also be strongly bound to the surface in order to prevent metal dissolution when exposed to an aggressive medium.[2] The copper protection by alkanethiol SAMs is the most investigated system of corrosion protection by long-chain organic molecules. For example, Laibinis and Whitesides[3] reported that alkanethiols adsorbed on copper surface are effective inhibitors of atmospheric copper corrosion. It was also demonstrated that alkanethiols inhibit atmospheric corrosion of copper, zinc and Cu-Zn alloys induced by formic acid,[4–7] as well as corrosion in aqueous solutions.[8–11] Due to the strong binding between sulfur and copper atoms, alkanethiol SAMs formed on non-oxidized copper surface have better protective properties compared to those formed on copper oxides.[11] In contrast to SAMs of alkanethiols, long-chain organic acids, such as carboxylic,[12–20] hydroxamic[15,21,22] or phosphonic[15,23–27] acids bind strongly to oxidized surfaces of metals and alloys, which is an advantage for their practical application as most of the commercially important metals and alloys readily get covered by thin oxide layers when exposed to air. The other advantage of long-chain organic acids, especially carboxylic acids is that they are non-toxic. Most of the studies on long-chain organic acids SAMs are focusing on characterization of SAM structure and binding of head group to metal surface[14,16] but there are far less studies that focus on efficiency and durability of corrosion protection provided by SAMs, especially on alloys. Studies on alkanethiols show that they provide good initial protection against atmospheric and aqueous corrosion but prolonged exposure to corrosive medium results in increased disorder in SAMs and oxidation of substrate.[3,4] Similar results were observed for alkanoic acids SAMs exposed to HCl vapor.[20] Additionally, highly organized stearic[19] or octadecylphosponic acid layers[27] are not stable in water because they are continuously lost through molecular desorption. For this reason, although many studies show that SAMs of long-chain organic acids provide excellent initial corrosion protection, stability of such protection should be verified as well. Another question is whether one monolayer is enough to ensure long-term stability or would thicker films, consisting of multiple layers provide better corrosion protection. Studies of Xing et al.[28] have shown that in the case of Langmuir-Blodgett monolayers of stearic acid, corrosion protection in neutral chloride medium increases with the number of deposited monolayers. Corrosion inhibition provided by the first monolayer was the most pronounced and was attributed to both blocking effect and negative catalysis effect, while the protection provided by outer layers was solely attributed to the blocking effect. Multilayers can also form by self-assembly upon longer exposure of the substrate to amphiphile solution or in solutions of higher concentration than those commonly used for SAM preparation (i.e. 1 mM).[29–31] As the number of layers increases, the intermolecular interactions within the layer become predominant in determining the properties of the layer.[32]

Our previous studies[17,18] showed that self-assembled films of stearic acid (SA) significantly increase corrosion resistance of copper-nickel alloys in seawater. It was also found that the thickness of stearic acid film increases with an increase of SA concentration. Thicker films more significantly hinder cathodic corrosion reactions by decreasing the diffusion of oxygen toward alloy surface. Still, better cathodic reaction hindrance did not necessarily result in higher reduction of overall corrosion rate, which was explained by formation of less homogeneous structure for thicker films. Films formed in 1 mM SA solution had a roughness similar to that of blank sample, and thus it was concluded that a monolayer was formed. However, ellipsometric measurements presented in this paper show that the thickness of such film is above the values expected for single monolayer. For that reason, in this work, the self-assembly procedure was modified in order to obtain a monolayer.

The aim of this paper is to examine the corrosion protection of self-assembled mono- and multilayers of stearic acid on copper-nickel alloy. We evaluated the contribution of the first monolayer chemisorbed on alloy surface as well as the contribution of upper layers to overall corrosion protection provided by self-assembled film in solutions resembling sea water. In other words, our goal is to examine if monolayer film provides sufficient protection to copper-nickel alloy or multilayer structure should be preferred.

## Experimental

***Sample preparation.—***Investigations were performed on cupronickel alloy (70Cu30Ni) obtained from Goodfellow Inc., UK. The specimens were cut-out from a cupronickel rod with a 1.3 cm diameter and 0.5 cm in thickness. In order to prepare working electrodes for electrochemical measurements on the back-side of these plates, a copper wire was soldered, and then the electrodes were embedded into epoxy resin. The exposed surface area of the working electrodes was 1.33 $cm^2$. The electrodes (or coupons for spectroscopic and microscopic measurements) were, prior to all investigations and/or

*Electrochemical Society Member.
[z]E-mail: helena.otmacic@fkit.hr; hosseinpour@mpip-mainz.mpg.de

surface treatment, abraded with emery paper grade 800, 1200, 2500, and polished with α-$Al_2O_3$ particle size 0.1 μm, degreased with ethanol in ultrasonic bath and rinsed with re-distilled water.

Stearic acid was obtained from Sigma-Aldrich Corp. USA and ethanol (EtOH) and tetrahydrofuran (THF) were obtained from Lachner d.o.o. Croatia. The SAM formation was carried out by the following procedure: oxide formation, 24 h at 80°C, followed by acid adsorption from EtOH (3 h and 20 h) or THF (3 h) solution of SA, at 40°C, and final drying step, 5 h at 50°C.[18] The use of THF, as a solvent besides ethanol, was motivated by studies that show that better quality layers form in solvents with lower dielectric constant.[33] However, since the epoxy resin can degrade in a prolonged contact with THF, a Teflon holder was used instead of epoxy resin for electrochemical measurements of samples with THF deposited SAMs. Finally, weakly bounded molecules were removed from the surface in two ways: the first set of samples was wiped with lens cleaning tissue soaked in ethanol and then rinsed with ethanol (wiped samples) while the second set of samples was just rinsed thoroughly with ethanol (non-wiped samples).

***Surface layer investigations.—***The surface topography was examined using a Multimode AFM with a Nanoscope IIIa controller (Bruker, Billerica, USA) with a vertical engagement 125 μm scanner (JV). Tapping mode imaging was performed under ambient conditions in air, by using silicon tips (RTESP, Bruker, nom. freq. 320 kHz, nom. spring constant of 42 N/m) and at a scan resolution of 512 pixels per line. The linear scanning rate was optimized between 1.0 and 2.0 Hz at a scan angle of 0°. Images were processed and analyzed by means of the offline AFM NanoScope software, versions 5.12r5 and 1.7. Roughness analysis software option was used to perform roughness analyses. The possible alteration of sample surface composition upon polishing has not been considered in this work since all the samples are polished in the same manner and thus their comparison is legitimate without evaluation of the exact surface composition.

Ellipsometric measurements were made using an AUTO EL IV ellipsometer at wavelengths of 830, 623.8 and 405 nm using a 70° angle of incidence at the sample. The results from these different wavelengths were not significantly different, thus only results at 623.8 nm are presented. Prior to the measurements of treated samples, the pseudo-optical constants of the blank sample (only oxide formation step conducted) were measured ($n = (1.58 \pm 0.03) + (3.36 \pm 0.03)\,i$) at 5 different points on the substrate. The 0.03 uncertainty is due to the inhomogeneity of the substrate itself and it translates to incertitude of 0.6 nm when measuring the thickness of thin films. Therefore all the subsequent measurements of film thicknesses have an intrinsic uncertainty of ± 0.6 nm due to the inhomogeneity of the substrate. The thickness values were calculated using the simple single-film model and fixed values for the optical constants ($n = 1.429$, $k = 0$) of the adsorbates which is an average value of many organic compounds.[30]

Contact angle measurements were performed in order to obtain information about the properties of the surface of the monolayer as well as the packing density. The water contact angle measurements (CA) on bare cupronickel and treated samples were performed using a goniometer DataPhysics Contact Angle System OCA 20, with a drop of 2 μL deionized water under the ambient atmospheric conditions. Contact angle measurements were performed on both samples mounted in epoxy and on samples without epoxy and no difference was observed between obtained results. This excludes the possibility of the incorporation of the contamination on the surface film.

***Sum frequency generation (SFG) investigations.—***An inherent surface sensitive tool, SFG was used to investigate the order and structure of formed SAMs. Principals of SFG and its applications in evaluating the SAMs structures on metals have been extensively described in the literature[34–37] and here only the relevant information is provided. In SFG spectroscopy, two laser pulses ($\omega_{IR}$ and $\omega_{vis}$) are spatially and temporally overlapped to generate the third beam, the SF beam, with its frequency equivalent to the sum of the frequencies of the incoming beams ($\omega_{SFG} = \omega_{IR} + \omega_{vis}$). Under the dipole approximation, the SFG process is forbidden in centrosymmetric media, such as the backbone of the all-trans hydrocarbons. At the surfaces or interfaces or at the gauche defects in the hydrocarbon chains where the symmetry is broken, SFG signal is generated.

In this study, the output of a commercial Ti:sapphire laser (800 nm, ∼47 fs, Coherent) was split in to two beams using a beamsplitter. To generate a broadband mid-IR beam in the CH region (2700–3000 $cm^{-1}$), the first beam was used to pump an optical parametric amplifier and non-collinear different frequency generation unit (TOPAS/NDFG). The second beam was spectrally narrowed passing through an Etalon and was used to up-convert the mid-IR beam through a sum frequency process. The broad mid-IR and narrow visible beams were spatially and temporally overlapped on the sample surface to generate the SFG signal. The emitted SFG signal was spatially and spectrally separated from the reflected incoming beams, was focused and dispersed by a monochromator, and detected by an electron-multiplying CCD. All three beams, mid-IR, visible and SFG were P-polarized to achieve the highest signal intensity.

There are two contributions in SFG signal: resonant and non-resonant. On metals, the resonant SFG signal from the adsorbates is interfering with the intense non-resonant signal generated from the metal making the interpretation of the SFG results difficult. In this study, the non resonant signal suppression method developed by Lagutchev[38] is used by delaying the visible and mid-IR beams by around 300 fs to overcome this difficulty. Such a non-resonant suppression method is ideal for qualitative studies of SAMs on metals, however extra care should be made for any quantitative interpretation and orientation analysis when nonresonant suppression method is employed.

***Electrochemical investigations.—***The electrochemical investigations were conducted in a three electrode cell, in a 3% NaCl solution. A platinum foil and saturated calomel electrode were used as the counter and reference electrode, respectively. All potentials in the text are referenced against saturated calomel electrode (SCE). Prior to electrochemical measurements the electrodes were immersed in the test solution for 1 hour to stabilize at the open circuit potential ($E_{oc}$).

The polarization measurements were performed at the wide (± 150 mV vs. $E_{oc}$) and narrow (± 20 mV vs. $E_{oc}$) potential ranges, with a potential scan rate of 0.166 mV $s^{-1}$. Corrosion current density ($j_{corr}$) was determined by Tafel extrapolation method while inhibiting efficiency ($\eta_i$) is calculated by Equation 1:

$$\eta_i = \frac{j_{corr,0} - j_{corr,i}}{j_{corr,0}} \times 100\% \qquad [1]$$

where $j_{corr,0}$ and $j_{corr,i}$ represent corrosion current densities of blank and treated sample respectively.

The electrochemical impedance spectroscopy (EIS) was performed at $E_{oc}$ in the frequency range of 100 kHz to 10 mHz with a 10 $mV_{rms}$ amplitude. The electrochemical measurements were performed using a Bio-Logic SP-300 potentiostat.

## Results

***Ellipsometry.—***The ellipsometric measurements were performed in order to determine the thickness of SA layers formed under various conditions. Table I illustrates that the thickness of the SA layer formed in 1 mM SA THF solution after 3 h of immersion is about 2.5 nm, which corresponds to the thickness of one monolayer.[16] When ethanol is used as a solvent, a thicker layer is formed, which corresponds to 2–3 monolayers. For samples prepared during 20 hours, the layer thickness is higher and corresponds to 3 and 7–8 monolayers for 0.1 mM SA and 1 mM SA samples, respectively. All these samples were rinsed with ethanol after the drying step, which indicates chemical stability of these layers. However, when additional force was applied, i.e. wiping with paper tissue soaked in ethanol, upper layers were removed, leaving only the first monolayer, chemically bonded to surface (1 mM SA EtOH 20 h wiped). Although the wiping procedure is not a common method to prepare SAMs, in this paper it was used

**Table I. Thickness of SA layers determined by ellipsometry.**

| Sample | layer thickness/nm (min-max. value) | expected monolayer number |
|---|---|---|
| 0.1 mM SA (20 h), in EtOH | 7–7.7 | 3 |
| 1 mM SA (20 h), in EtOH | 16.4–20.3 | 7–8 |
| 1 mM SA wiped (20 h), in EtOH | 2.4–3.0 | 1 |
| 1 mM SA (3 h), in EtOH | 5.2–7.9 | 2–3 |
| 1 mM SA (3 h), in THF | 2.5–3.6 | 1 |

**Table II. The water contact angle for wiped and non wiped samples.**

| Sample | Contact angle / ° |
|---|---|
| Blank CuNi | 60 ± 3 |
| 0.1 mM SA (20 h), in EtOH | 108 ± 1 |
| 1 mM SA (20 h), in EtOH | 112 ± 2 |
| 1 mM SA wiped (20 h), in EtOH | 103 ± 1 |
| 1 mM SA (3 h), in EtOH | 105 ± 1 |
| 1 mM SA (3 h), in THF | 103 ± 2 |

to verify whether the first layers of stearic acid, adsorbed directly on the metallic surface, are more strongly bonded to the surface than upper layers. Raman et al.[12] have similarly examined that monolayers of alkanoic acids, on stainless steel were resistant to rinsing and sonication if preparation procedure involved drying step at elevated temperatures, while without the overnight annealing step monolayers were easily removed.

***AFM.***—AFM studies (Figure 1a) show that roughness of 1 mM SA layer is similar ($R_a = 2.20$ nm) to that of a nontreated sample ($R_a = 2.42$ nm).[17] Raman et al.[12] have concluded that if the roughness of the modified surface is similar to that of the bare surface, then the sample is considered to be covered by film of the monolayer height that follows the contour of the surface. In our case, ellipsometry showed the formation of a multilayer structure. As the roughness of the film is only slightly lower than that of the blank sample, one may assume that the multilayer SA film is compact and with a small number of defects. After wiping, the surface of stearic acid treated sample maintains similar roughness, except for the part where the wiped layer has plugged the polishing lines of the surface (Figure 1b). In order to check if the wiping procedure resulted in complete layer removal, contact angle and SFG measurements were performed on both wiped and non wiped samples.

Surface wettability has been shown to be useful tool for estimating the monolayer quality. Densely packed and well-ordered monolayers predominantly expose methyl groups at the surface and decrease the surface wettability. However, loosely packed monolayers expose both methyl and methylen groups at the surface which results in increased wettability.[12] Contact angle measurements (Table II) show that all surfaces treated with stearic acid have hydrophobic properties, i.e. contact angle above 100°. In our previous work,[17] the contact angles obtained for 1 mM SA showed slightly lower values (around 103°),

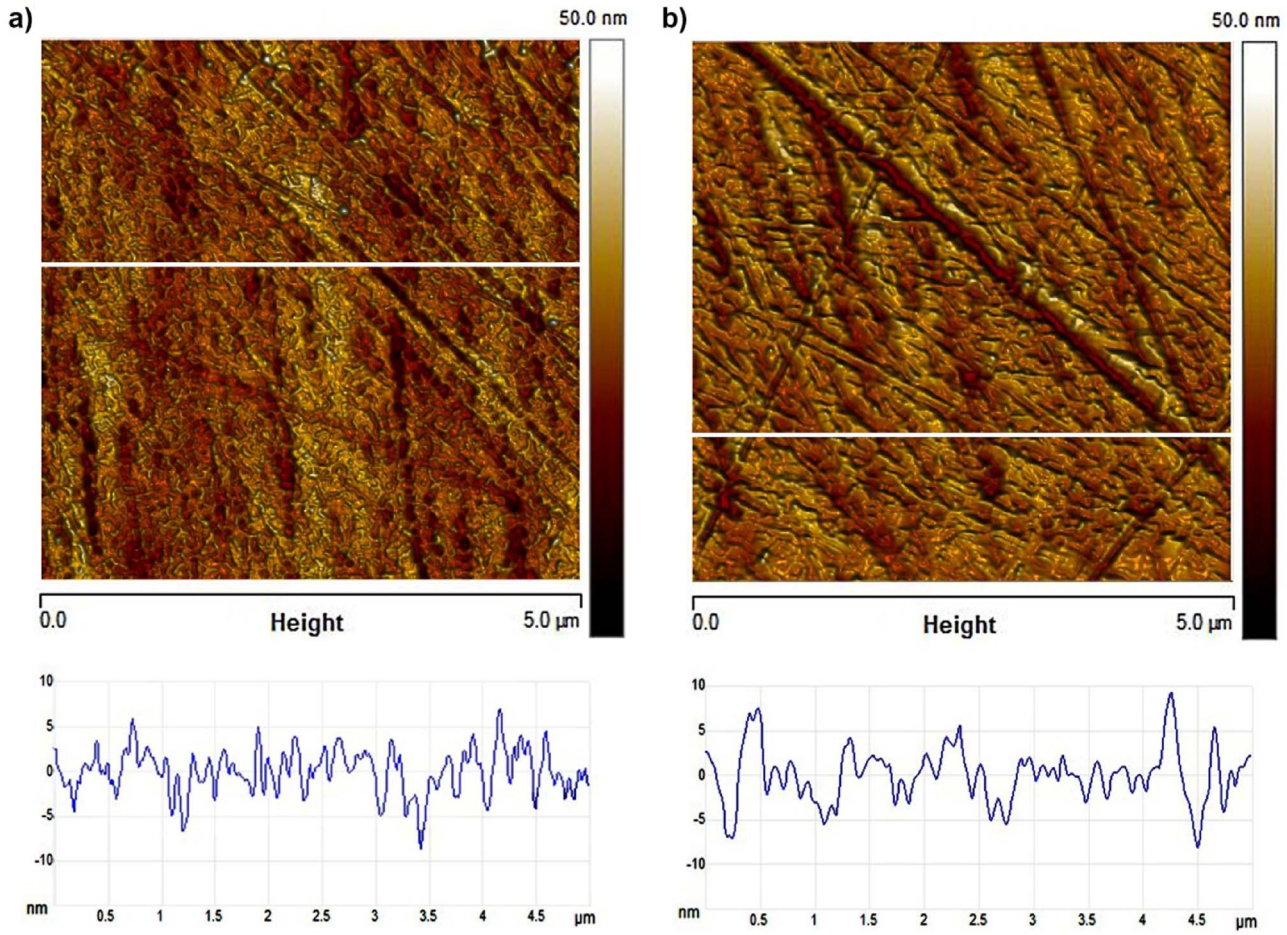


**Figure 1.** Surface topography of sample modified in 1 mM stearic acid a) before and b) after wiping (scan size 5 µm × 5 µm, vertical scale 50 nm) and corresponding section analysis.

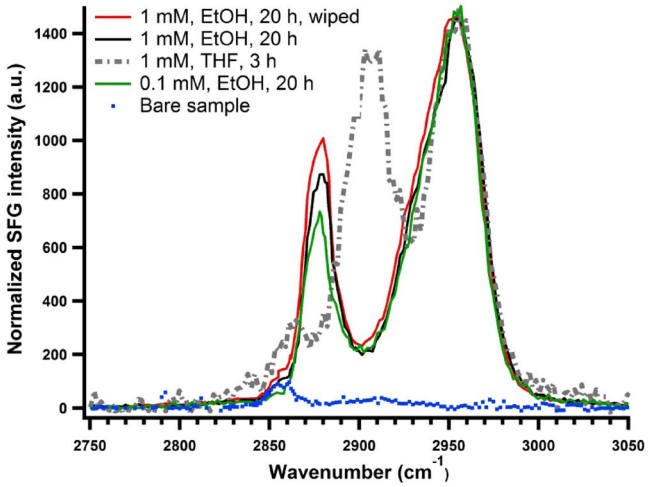


**Figure 2.** Normalized SFG spectra of SA layer deposited on Cu-Ni alloy from ethanol (continues lines) and THF (dotted line) as solvent. All spectra are normalized for the intensity of the $CH_3$ asymmetric peak at ~2960 $cm^{-1}$.

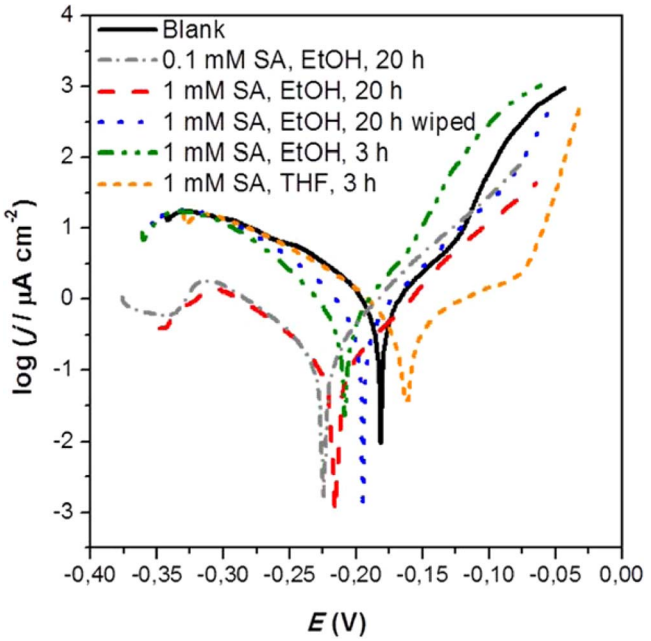


**Figure 3.** Polarization curves for SA treated samples.

which was probably caused by longer storage period of the samples before the measurement as the contact angle decreases in time.[16] After wiping, contact angle decreases to a value close to the contact angle of the 3 h 1 mM SA sample. To prove that examined layers are well ordered, SFG measurements were conducted.

***SFG.***—Figure 2 shows the SFG results obtained on SA layers deposited in ethanol and THF as well as on a blank sample in the CH stretching vibration region (i.e. ~2700–3000 $cm^{-1}$). As explained earlier, the non-resonant suppressed spectra can be used, with no ambiguity due to the interference with the non-resonant signal, to determine the degree of the order in the formed layer. The SFG spectra on SA layers deposited from ethanol for 20 h with both 0.1 mM and 1 mM concentration (before and after wiping) consist of vibrations from terminal $CH_3$ groups. These modes include $CH_3$ symmetric vibration at ~2880 $cm^{-1}$, $CH_3$ asymmetric vibration at ~2960 $cm^{-1}$ and the Fermi resonance of the bending overtone and stretching mode at ~2940 $cm^{-1}$, which appears as a shoulder next to the $CH_3$ asymmetric mode. In these spectra, the contribution of the $CH_2$ vibrations, expected at ~2860 $cm^{-1}$ for the $CH_2$ symmetric and ~2915 $cm^{-1}$ for the $CH_2$ assymmetric, is barely observed, which is an indication of relatively well ordered all-trans layers of SA with very small contribution of gauche defects in their structure. It should be noted that the area in which the SFG signal is collected is relatively big and thus the information obtained by SFG spectroscopy is average information of the probed area. For a more detailed investigation of local variations in the structure of these layers, SFG imaging with lateral resolution of sub-micron is very advantageous.[39] The SFG spectrum of the SA layer deposited in THF clearly shows the appearance of the $CH_2$ asymmetric peak, at ~2915 $cm^{-1}$ indicating the less ordered structure of this layer accompanied with the increased intensity of the $CH_2$ symmetric peak, at ~2860 $cm^{-1}$. Combined with the results from ellipsometric measurements, it can be concluded that organization of the SA layer formed in a more polar solvent, i.e. THF, is poor compared to that formed in a less polar solvent, i.e. ethanol.

Considering the fact that all samples, independent of layer thickness, show hydrophobic properties, and SFG measurements confirm the presence of an ordered layer, one may assume that the structure of SA films with thickness bigger than 2.5 nm consist of one monolayer chemisorbed on the copper nickel surface on top of which assemble additional SA layers. In the outermost layer the hydrophobic part of SA molecule (i.e. $CH_3$ group) is pointing outwards, making the surface hydrophobic. This is in agreement with the research performed by Nie et al.[31] who have studied the structure of octadecylphosponic acid layers on Si. They have observed the formation of large area bilayer and odd-numbered multilayers after heat-treatment of the samples at 50–60°C (such treatment is also applied in our study). They have concluded that a hydrophobic tail terminated surface is more favorable than a hydrophilic headgroup terminated surface. Additionally, Sato et al.[40] have observed formation of hydrophobic multilayer films of tetradecyl phosphonic acid after assembly at room temperature on anodized aluminum.

***Electrochemical measurements.***—The results given above show that depending on SA concentration and adsorption time, SA layers of different thickness are formed. The electrochemical measurements were performed in 3% NaCl in order to determine barrier properties and corrosion protection offered by such films. Polarization curves recorded after one hour immersion of blank and treated samples in chloride solution are presented in Figure 3. Table III presents the corrosion parameters, corrosion potential ($E_{corr}$), corrosion current density ($j_{corr}$), anodic and cathodic Tafel slopes ($b_a$ and $b_c$), obtained from the polarization curves by Tafel extrapolation method.

The results show that for 20 h treated samples corrosion current density significantly decreases compared to that of the blank sample. The protective film acts as a barrier toward oxygen diffusion, thus slowing down cathodic corrosion reaction, while anodic corrosion reaction decreases to a lesser extent. After wiping the 1 mM SA sample, increase of current densities is observed, indicating less efficient protection of alloy. As previous measurements (ellipsometry, SFG, contact angle) showed, after wiping an ordered monolayer of stearic acid remains on copper-nickel surface, therefore it is obvious that barrier properties of upper SA layers, which are removed by wiping, have significant impact on corrosion protection offered by the SA film. It may be argued that this effect can be explained by the formation of local defects in the SAMs due to the wiping, despite the fact that SFG showed presence of well ordered layer. For that reason, our attempt was to prepare a single layer of SA on copper-nickel surface also by methods other than wiping.

In the literature, different deposition times and solvents are used for preparation of well ordered and compact self-assembled monolayers of carboxylic acids. For example, Tao[17] applied dip coating in 1 mM solutions of alkanoic acids in *n*-hexadecane during 3 h, while Raman[15] applied 2 h dip coating in 1 mM THF solution. We chose to apply 3 h dip coating in 1 mM SA dissolved in THF and ethanol. Ellipsometric measurements (Table I) showed that a single monolayer was

**Table III. Corrosion parameters determined by Tafel extrapolation method from polarization curves given in Figure 2. Values in parenthesis represent standard deviation.**

| | Sample | $E_{corr}$ (mV) vs.SCE | $j_{corr}$ ($\mu$A cm$^{-2}$) | $b_a$ (mV dec$^{-1}$) | $-b_c$ (mV dec$^{-1}$) | $\eta_i$ (%) |
|---|---|---|---|---|---|---|
| | Blank | −177 (6) | 1.12 (0.10) | 78 (21) | 95 (5) | - |
| EtOH 20 h | 0.1 mM SA | −214 (22) | 0.24 (0.07) | 65 (7) | 74 (23) | 78 |
| | 1 mM SA | −201 (12) | 0.09 (0.02) | 50 (2) | 79 (16) | 92 |
| | 1 mM SA wiped | −181 (14) | 0.46 (0.06) | 69 (28) | 79 (15) | 58 |
| EtOH 3 h | 1 mM SA | −212 (5) | 0.37 (0.05) | 43 (1) | 53 (1) | 67 |
| THF 3 h | 1 mM SA | −170 (13) | 0.37 (0.02) | 55 (13) | 66 (11) | 67 |

formed only in THF. Polarization measurement conducted on samples treated with THF solution (Fig. 3 and Table III) show that mostly the anodic corrosion reaction was slowed down. It may be assumed that the SA has adsorbed on anodic sites of alloy thus preventing their dissolution. On the other hand, cathodic corrosion reaction was not much influenced by the presence of SA layer, so it can be concluded that SA cannot efficiently prevent diffusion of water and $O_2$ toward the copper-nickel surface due to its disordered structure as seen by SFG. Interestingly, when adsorption was conducted in ethanol solution during 3 h, an ordered film was formed (Figure 2), which then reflects in more pronounced cathodic reaction inhibition compared to sample prepared in THF solution. Still, inhibiting efficiency for both samples (Table III) was more or less the same as the latter sample exhibits lower anodic current densities.

In order to better understand the corrosion behavior of studied samples, EIS measurements were performed. EIS spectra obtained for different samples after one hour of immersion in chloride medium are given in Figure 4. It can be readily seen that impedance modulus ($|Z|$) at the lowest frequencies is the highest for the thicker samples, i.e. multilayer film prepared in 1 mM SA EtOH solution for 20 h. The impedance modulus is about three times lower for the sample with approximately three times thinner SA layer prepared in and 0.1 mM SA for 20 h. Although ellipsometry showed that that the film formed in 1 mM SA EtOH solution for 3 h has thickness of approximately 2 monolayers, its impedance spectra are almost the same as those of sample covered by monolayer (1 mM SA THF 3 h). If a compact and defect free two layer film had formed, the surface of 1 mM SA EtOH 3 h sample would be hydrophilic but contact angle measurements (Table II) showed that surface became hydrophobic. Based on these findings we can assume that, due to short adsorption time, above the first well ordered monolayer (as shown by SFG), upper layers have more defects and do not particularly contribute to overall corrosion protection.

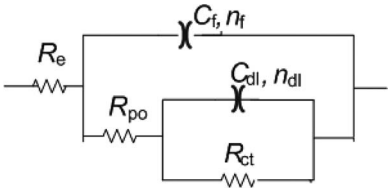


**Figure 5.** Equivalent electrical circuit used for fitting the EIS spectra.

For fitting the impedance data given in Figure 4, the equivalent circuit shown in Figure 5 was used. In order to accurately fit the spectra, two time constants were necessary. Proposed 2RC circuit (Figure 5) used for fitting EIS spectra consists of $R_{po}$ – $C_f$ and $R_{ct}$ – $C_{dl}$ couples. $R_{po}$ – $C_f$ couple describes a time constant observed at high frequencies, where $R_{po}$ corresponds to the resistance of the pores in the film and the $C_f$ to the capacitance of the surface film associated with the dielectric property of this film. $R_{ct}$ – $C_{dl}$ couple presents the corrosion reaction at the metal substrate/solution interface, where $R_{ct}$ is charge transfer resistance and $C_{dl}$ is double layer capacitance. The electrolyte resistance between the working and reference electrodes is represented by $R_{el}$.

Due to the frequency dispersion, capacitive elements in real electrochemical systems are usually represented by constant phase

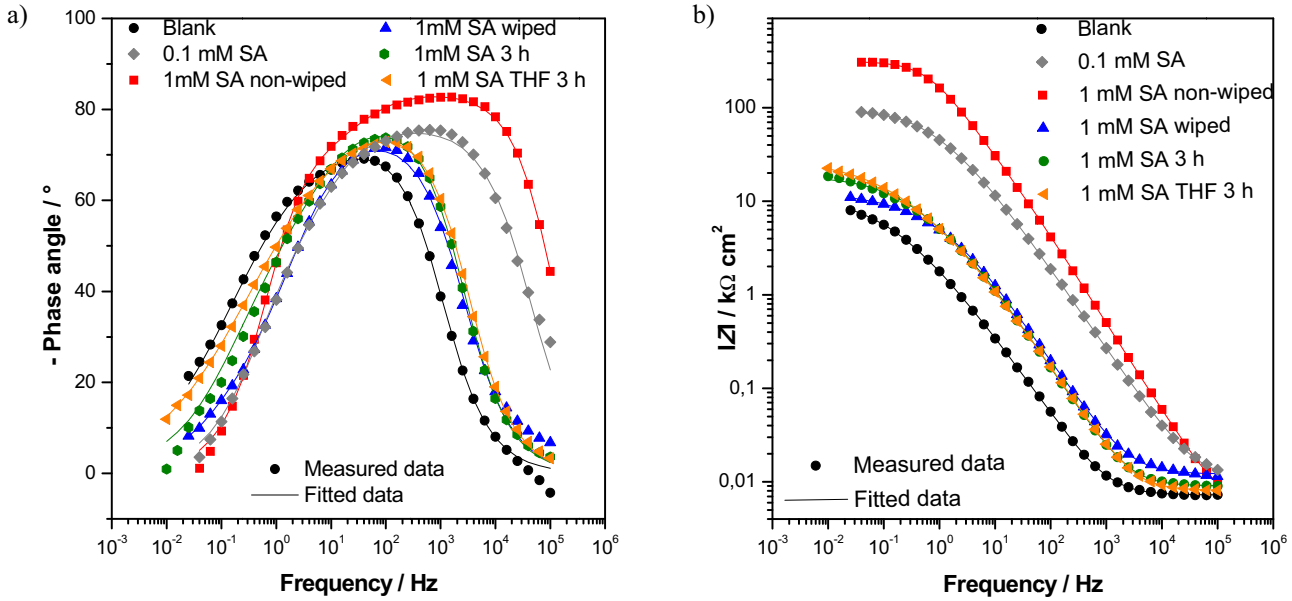


**Figure 4.** Bode plots of EIS spectra for SA treated samples: a) phase angle, b) impedance modulus. Dots present experimental data and lines fitted data obtained by fitting the spectra to model given in Figure 5.

**Table IV. Impedance parameters obtained by fitting experimental data to selected equivalent circuits. Values in parenthesis represent standard deviation.**

| | | $C_f$ / μF cm$^{-2}$ | $n_f$ | $R_{po}$ / kΩ cm$^2$ | $C_{dl}$/μF cm$^{-2}$ | $n_{dl}$ | $R_{ct}$/kΩ cm$^2$ |
|---|---|---|---|---|---|---|---|
| | Blank | 47.70 (10.1) | 0.86 (0.00) | 3.08 (2.50) | 434.60 (67.68) | 0.53 (0.04) | 6.60 (4.86) |
| EtOH 20 h | 1 mM SA non-wiped | 0.88 (0.73) | 0.86 (0.13) | 61.13 (19.73) | 0.27 (0.02) | 0.78 (0.04) | 242.45 (23.55) |
| | 1 mM SA wiped | 22.20 (6.52) | 0.85 (0.01) | 5.59 (0.70) | 154.00 (50.70) | 0.72 (0.14) | 5.32 (1.48) |
| | 0.1 mM SA | 4.42 (3.07) | 0.87 (0.02) | 18.30 (16.01) | 9.60 (8.17) | 0.68 (0.03) | 29.10 (23.88) |
| EtOH 3 h | 1 mM SA | 11.00 (5.41) | 0.88 (0.01) | 3.70 (1.04) | 18.00 (12.95) | 0.52 (0.04) | 13.70 (0.38) |
| THF 3 h | 1 mM SA | 9.51 (4.46) | 0.87 (0.01) | 3.06 (2.30) | 34.60 (30.44) | 0.50 (0.00) | 19.70 (6.77) |

element CPE.[41] The impedance of CPE is defined as

$$Z(\text{CPE}) = \frac{1}{Q(j\omega)^n} \quad [2]$$

where $Q$ is the constant of the CPE element, $j$ imaginary number, ω is the angular frequency, and $n$ is the CPE exponent where $-1; \leq n \leq 1$. The value of $n$ is associated with the non-uniform distribution of current as a result of roughness and surface defects. The $n$ values of nearly one suggest nearly ideal capacitive behavior. According to Brug et al.[42] the value of pseudocapacitance $C$ can be calculated using relationship $C = (QR_b^{1-n})^{1/n}$.

The impedance parameters obtained by fitting the EIS data to equivalent circuits are presented in Table IV.

The parameters given in Table IV show that film capacitance values ($C_f$) of 0.1 mM SA sample are 4 times higher than those obtained for 1 mM SA (both prepared in EtOH during 20 h), which confirms that in the latter case thicker layer was formed, as observed by ellipsometric measurements (Table I). For samples prepared by 3 h adsorption film capacitance is more than 10 times lower, compared to the sample with the thickest layer, which can be explained by both decreased layer thickness and a significant water diffusion into the layer. Accordingly, $R_{po}$ decreases from thicker to thinner layer covered samples.

AFM measurements (Figure 1b) showed that on wiped samples remnants of the thicker layer may plug polishing lines which could explain why this sample has higher film resistance than the 1 mM SA 3 h THF sample of approximately same thickness. The $R_{ct}$ values decrease with the decrease of the layer thickness (1 mM SA > 0.1 mM SA> 1 mM SA 3 h THF). For 1 mM SA 3 h EtOH sample $R_{ct}$ values are even lower. The lowest $R_{ct}$ and the highest $C_{dl}$ values were observed on wiped samples. This is a sign that the protective monolayer was partially removed by wiping procedure. Such conclusion is not in a contradiction with results showing well ordered structure of SA layer on wiped sample. Lim et al.[19] have, for example, noticed that during the desorption of stearic acid on $Al_2O_3$ surface into water, surface coverage decreases but the alkyl chain packing order within the remaining islands is maintained. The observed order of $R_{ct}$ values agrees well with order of $j_{corr}$ vales given in Table III.

In order to evaluate stability of the prepared mono and multilayers of stearic acid, samples were exposed to a chloride medium for several days. Polarization resistance evolution in time is presented in Figure 6. The best results were observed for the thickest layer (1 mM SA, EtOH 20 h) and more importantly polarization resistance of that sample did not decrease with time. For thinner film (0.1 mM SA, EtOH 20 h), lower polarization resistance is observed but its value is also almost constant in time. The $R_p$ values for other three samples initially show the same order as impedance modulus at the lowest frequencies, i.e. the highest value is obtained for 1 mM SA THF 3 h sample. However, after 2 days of immersion, the $R_p$ value of the sample prepared in THF decreases and becomes the same as that of the unprotected copper-nickel sample. The SFG results have shown less ordered structure of monolayer formed on this sample which is the probable cause of its fast deterioration. Moreover, the wiped sample and the one prepared in ethanol for 3 h initially show lower $R_p$ values but they increase slightly in time and stay higher than $R_p$ values of blank sample. Interestingly, the other three samples prepared in ethanol also show increase of $R_p$ after 3 days of immersion in a chloride solution. Thus, some degrees of reorganization of molecules in the SA layer upon the exposure to chloride medium are proposed, which leads to better protection. For thinner SA layers, oxidation of substrate can also result in increase of $R_p$ value[27] as it is the case for blank sample.

***AFM studies in time.***—Results presented in this work show that, if ordered and compact multilayers of stearic acid are formed, they can provide better corrosion protection to underlying alloy than a single self-assembled monolayer. This may be explained by formation of more efficient diffusion barrier. However, our previous work[17] showed that thicker layers formed in more concentrated solutions did not necessarily provide better corrosion protection. This contradiction can be explained by AFM imaging of the sample prepared in $10^{-2}$ M SA EtOH solution during 20 h under influence of the 3% NaCl. The effect of the corrosion process is clearly demonstrated in the cross section analysis of the sample before and after 1 h immersion in a chloride medium. The typical 3D topographic view of the sample before (Figure 7b) and after 1 h exposure to 3% NaCl (Figure 7c) obtained by the AFM imaging in this study reveal rougher surface after exposure with several high region with pointed peaks emerging perpendicularly from the surface. Moreover, deeper holes within the film can be observed compared to the initial state (Fig. 7a) resulting in the increase of the roughness. Roughness analysis revealed that the roughness value ($R_a$) is lower at initial state ($R_a = 6.2 \pm 0.3$ nm) than after immersion ($R_a = 8.8 \pm 0.5$ nm). These results are in agreement with other studies[43] examining the dissolution of long chain organic acid monolayers, showing that desorption of molecule from the monolayer/hole boundary is significantly more likely than from a continuous region of monolayer. On the other hand, the sharp edges of the film have been smoothed by

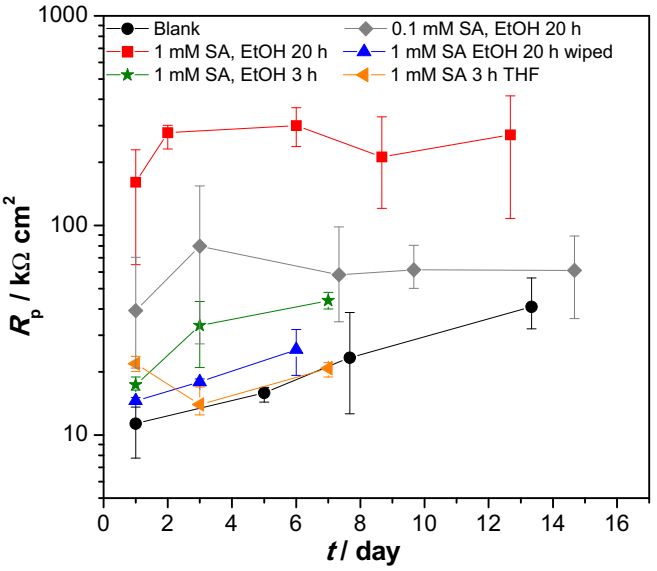


**Figure 6.** Polarization resistance dependence on time of exposure to chloride medium

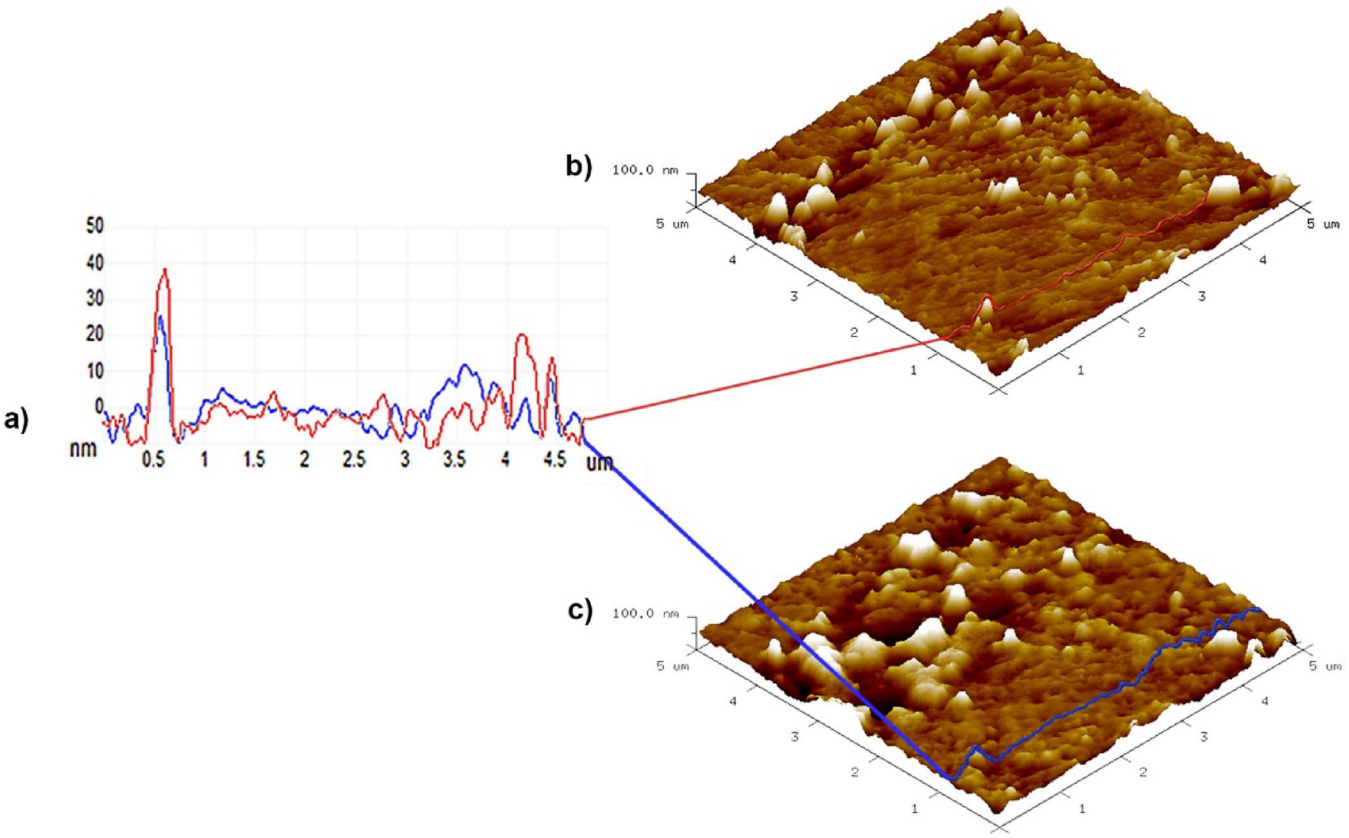


**Figure 7.** AFM images of $10^{-2}$ M SA sample a) surface profiles for the same position on the surface-$t_0$ –red line, $t_1$-blue line b) 3D topographic view before immersion in 3% NaCl ($t_0$) and c) after 1 h of immersion ($t_1$) with marked lines where surface profiles were measured.

exposure to 3% NaCl and the material from the upper layer is removed on the other place. Thissen et al.[27] have shown that octadecyl phosponic acid (ODPA) molecules can dissolve into the aqueous phase but due to the low solubility they immediately form a second layer on the pre-existing SAM and stay physisorbed.

Based on results presented in this paper, it can be concluded that only compact layers significantly contribute to stable and efficient corrosion protection of a substrate, while defective layers are porous and dissolve more easily thus weakly contributing to corrosion protection efficiency. In this work, corrosion protection by SA layers was examined on a polycrystalline alloy substrate that is not perfectly smooth and homogenous. For that reason, it may be expected that the monolayer formed on such substrate could have defects in the structure. Therefore, excellent corrosion inhibition by one monolayer is much harder to achieve than on single crystalline or perfectly flat substrates.

It has to be stressed that SAM preparation procedure, used in this work, involves drying step at elevated temperatures. It was previously shown[18] that this step is crucial for preparation of homogenous SA layer. Heating may also enhance formation of bilayer structures similar to those in bulk SA.[31] Such layers are inverse of bilayers found in lipid membranes, where additional intermolecular and electrostatic interactions contribute to the enhanced stability and compactness of the film.[44] However, further studies are needed to determine the exact structure of the films.

## Conclusions

Results presented in this work show that self-assembled mono- and multilayers of stearic acid provide corrosion protection to copper-nickel alloy in a chloride medium. The corrosion protection increases with the number of SA layers, but only if compact, defect free structures, are formed. Films of only 17 nm thickness have excellent stability in water medium and cannot be easily removed by rinsing with ethanol. The thickness of the protective film depends on the deposition time and concentration of stearic acid (1 mM SA 3 h $<$ 0.1 mM SA 20 h $<$ 1 mM SA 20 h). The choice of solvent is also an important factor, which determines the structure and stability of stearic acid layer.

Studies performed in this work show that for the purpose of long lasting corrosion protection of copper nickel alloy, instead of monolayer films of stearic acid, ordered multilayer films should be applied.

## Acknowledgments

The research leading to these results has received funding from Croatian Science Foundation under grant agreement 9.01/253.

Financial support of German Academic Exchange Service (DAAD) project-ID 57141691 and Croatian Ministry of Sciences and Sports under bilateral German-Croatian exchange program is gratefully acknowledged.

## References

1. A. R. Bishop and R. G. Nuzzo, *Curr. Opin. Colloid Interface Sci.*, **1**, 127 (1996).
2. M. Rohwerder, M. Stratmann, and G. Grundmeier in *Corrosion Mechanisms in Theory and Practice*, P. Marcus (ed), p.617, CRC Press, Francis Taylor Group, USA (2012).
3. P. E. Laibinis and G. M. Whitesides, *J. Am. Chem. Soc.*, **114**, 9022 (1992).
4. S. Hosseinpour, M. Gothelid, C. Leygraf, and C. Magnus Johnson, *J. Electrochem. Soc.*, **161**, C50 (2014).
5. M. Forslund, J. Pan, S. Hosseinpour, F. Zhang, M. Johnson, P. Claesson, and C. Leygraf, *Corrosion*,. **71**, 908 (2015).
6. S. Hosseinpour, C. M. Johnson, and C. Leygraf, *J. Electrochem. Soc.*, **160**, C270 (2013).
7. S. Hosseinpour, M. Forslund, C. Magnus Johnson, J. Pan, and C. Leygraf, *Surf. Sci.*, **648**, 170 (2016).
8. Y. Q. Feng, W. K. Teo, K. S. Siow, Z. Q. Gao, K. L. Tan, and A. K. Hsieh, *J. Electrochem. Soc.*, **144**, 55 (1997).

9. Y. Yamamoto, H. Nishihara, and K. Aramaki, *J. Electrochem. Soc.*, **140**, 436 (1993).
10. G.Kane Jennings and Paul E. Laibinis, *Colloids Surfaces A: Physochem. Eng. Aspects* **116**, 105 (1996).
11. M. Metikoš-Huković, R. Babić, Ž. Petrović, and D. Posavec, *J. Electrochem. Soc.*, **154**, C138 (2007).
12. A. Raman and E. S. Gawalt, *Langmuir*, **23**, 2284 (2007).
13. I. Škugor Rončević Z.Grubač, M. Metikoš-Huković, R. Babić, M. Petravić, and R. Peter, *J. Electrochem. Soc.* **159**, C253 (2012).
14. D. L. Allara and R. G. Nuzzo, *Langmuir*, **1**, 45 (1985).
15. A. Raman, R. Quinones, L. Barriger, R. Eastman, A. Parsi, and E. S. Gawalt, *Langmuir*, **26**, 1747 (2010).
16. Y. T. Tao, *J. Am. Chem. Soc.* **115**, 4350 (1993).
17. Z. Hajdari, H. Otmačić, Ćurković, V. Čadež, and S. Šegota, *J. Electrochem. Soc.*, **163**, C145 (2016).
18. K. Marušić, Z. Hajdari, H. Otmačić, and Ćurković, *Acta Chim. Slov.*, **61**, 328 (2014).
19. M. S. Lim, K. Feng, X. Chen, N. Wu, A. Raman, J. Nightingale, E. S. Gawalt, D. Korakakis, L. A. Hornak, and A. T. Timperman, *Langmuir*, **23**, 2444 (2007).
20. Y.-T. Tao, G. D. Hietpas, and D. L. Allara, *J. Am. Chem.Soc.*, **118**, 6724 (1996).
21. J. Telegdi and E. Kalman T.Rigo, *J. Electroanal. Chem.*, **582**, 191 (2005).
22. J. Telegdi and H. Otmačić; K. Marušić Ćurković, F. Al-Taher, E. Stupnišek-Lisac, and E. Kalman, *Chem. Biochem. Eng. Q.*, **21**, 77 (2007).
23. K. M. Kruszewski, E. R. Renk, and E. S. Gawalt, *Thin Solid Films*, **520**, 4326 (2012).
24. G. Fonder, I. Minet, C. Volcke, S. Devillers, J. Delhalle, and Z. Mekhalif, *Appl. Surf. Sci.*, **257**, 6300 (2011).
25. Ž. Petrović, J. Katić, M. Metikoš-Huković, H. Dadafarin, and S. Omanovic, *J. Electrochem. Soc.*, **158**, F159 (2011).
26. J. Cabrita, A. S. Viana, and L. M. Abrantes, *Corros. Prot. Mater.*, **29**, 114 (2010).
27. P. Thissen, M. Valtiner, and G. Grundmeir, *Langmuir*, **26**, 156 (2010).
28. W. Xing, Y. Shan, D. Guo, T. Lu, and S. Xi, *Corrosion*, **51**, 45 (1995).
29. Y-T. Kim, R. L. McCarely, and A. J. Bard, *Langmuir*, **9**, 1941 (1993).
30. H. Keller, P. Simak, W. Schrepp, and J. Dembowski, *Thin Solid Films*, **244**, 799 (1994).
31. H.-Y. Nie, M. J. Walzak, and N. S. McIntyre, *Langmuir*, **18**, 2955 (2002).
32. X. Chen, E. Luais, N. Darwish, S. Ciampi, P. Thoardarson, and J. J. Gooding, *Langmuir*, **28**, 9487 (2012).
33. M. de Pauli, M de Castro Prado, M. J. Souza Matos, G. Noguiera Fontes, C. A. Perez, M. S. Carvalho Mazzoni, B. R. Almeida Neves, and A. Malachias, *Langmuir*, **28**, 15124 (2012).
34. C. D. Bain, *J. Chem. Soc., Faraday Trans.*, **91**, 1281 (1995).
35. Y. R. Shen, *Nature*, **337**, 519 (1989).
36. X. D. Zhu, H. Suhr, and Y. R. Shen, *Phys. Rev. B* **35**, 3047 (1987).
37. S. Hosseinpour, J Hedberg, S Baldelli, C Leygraf, and M Johnson, *J. Phys. Chem. C*, **115**, 23871 (2011).
38. A. Lagutchev, S. A. Hambir, and D. D. Dlott, *J. Phys. Chem. C*, **111**, 13645 (2007).
39. M. Fang and S. Baldelli, *J. Phys. Chem. Lett.*, **6**, 1454 (2015).
40. H. Sato, T. Fujii, E. Tsuji, Y. Aoki, K. Shimizu, P. Skeldon, G. E. Thompson, and H. Habazaki, *Surf. Interface Anal.*, **45**, 1441 (2013).
41. J. R. Macdonald, *Impedance spectroscopy: Emphasising Solid Materials and Systems*, John Wiley & Sons, New York (1987).
42. G. J. Brug, A. L. G. van der Eeden, M. Sluyters-Rehbach, and J. H. Sluyters, *J. Electroanal. Chem.* **176**, 275 (1984).
43. I. Doudevski and D. K. Schwartz, *Langmuir*, **16**, 9381 (2000).
44. S. Šegota, D. Vojta, G. Pletikapić, and G. Baranović, *Chem. Phys. Lipids*, **186**, 17 (2015).